RJC

RASĀYAN *J. Chem.*
Vol. 18 | No. 3 |1316-1323| July-September | 2025
ISSN: 0974-1496 | e-ISSN: 0976-0083 | CODEN: RJCABP
http://www.rasayanjournal.com
http://www.rasayanjournal.co.in

ZnO THIN FILMS PROPERTIES MODIFIED BY BN-DOPED VIA SOL-GEL SPIN COATING TECHNIQUE

Nurdin Siregar✉, Motlan and Makmur Sirait
Department of Physics, Faculty of Mathematics and Natural Sciences, Universitas Negeri Medan, Medan 20221, Indonesia
✉Corresponding author: siregarnurdin@unimed.ac.id

ABSTRACT

In this study, pristine and boron nitride (BN)-doped ZnO thin films were synthesized via the sol-gel spin coating technique to investigate their structural, morphological, and optical properties for application as photoanodes in Dye-Sensitized Solar Cells (DSSCs). XRD confirmed the hexagonal wurtzite structure, with defect-induced structural distortions appearing at higher B doping concentrations. Increasing B doping concentration led to a decrease in crystal size from 37.5 nm to 26.7 nm, accompanied by a significant surface transformation into a worm-like structure surrounded by flake-like features. EDS confirmed the presence of Zn and O peaks, while the low-intensity B peaks were attributed to weak X-ray signals and low B content. SEM revealed an increase in surface roughness with higher doping concentration which affects optical properties. The calculated optical band gap decreased from 3.37 eV to 3.28 eV, possibly due to increased defect states and lattice distortion. The results highlight the role of B doping in modifying properties, with ZOB-1 achieving the highest efficiency of 1.91% in DSSC application.

Keywords: ZnO Thin Films, BN-Doped, Doping Concentration, Sol-Gel Spin Coating Technique, Modified Properties, DSSC Application.

RASĀYAN *J. Chem.*, Vol. 18, No. 3, 2025

INTRODUCTION

One of the appealing materials for use in the fields of sensors, solar cells, materials engineering, nanodevices, and thin films is zinc oxide (ZnO). This material has valuable applications due to its unique emission characteristics, such as near-ultraviolet emission and having high conductivity with good transparency, which is good for photocatalysis.[1] ZnO is part of the semiconductor materials that belong to the II-IV compounds group because it has a band gap value of 3.37 eV and an exciton binding energy value of 60 meV at room temperature.[2,3] ZnO is frequently doped with extrinsic dopants, which are different elements that are replaced into the ZnO structure to improve its optical, electrical, and physical properties (e.g., B, Al, Ga).[4,5] Boron was selected as a doping element due to its large effective nuclear charge (Z), low ionic radius (r_R), and high (Z/r_R^2) value of 17.85, which allows it to polarize electrons more strongly than oxygen.[6] The boron dopant is considered useful in improving the electrical characteristics of ZnO and has the highest electronegativity value of 2.04, due to its short ionic radius (0.23 Å), which allows it to substitute for interstitial boron in the ZnO lattice. Various thin film deposition techniques have been developed, including spray pyrolysis,[7] chemical vapor deposition (CVD),[8] electrochemical deposition or electroplating,[9] RF magnetron sputtering or physical vapor deposition (PVD),[10] etc. Nevertheless, these techniques require intricate procedures that are performed on advanced machinery. However, the sol-gel spin coating method achieves a homogenous composition, controllable layer thickness, good microstructure, low synthesis temperatures, and the absence of a high vacuum chamber.[11,12] Studies on pristine ZnO films with boron nitride (BN)-doped have been conducted in several ways. A previous report successfully synthesized B-doped zinc acetate dihydrate, confirming a reduction in crystal size.[13] However, further investigation is needed to understand how different B doping concentrations influence the crystal structure, surface morphology, and optical properties of ZnO thin films. In this study, we synthesized ZnO thin films with various BN doping concentrations using the reflux method to form sol-gel and deposit the gels on indium tin oxide (ITO)-coated glass substrate with the spin coating technique. We systematically analyzed the effects of BN doping on the structural, morphological, optical, and electrical properties in order to evaluate their potential for solar cell applications.

http://doi.org/10.31788/RJC.2025.1839295
This work is licensed under a CC BY 4.0 license.

EXPERIMENTAL

Materials

Zinc acetate dihydrate [$Zn(CH_3COOH).2H_2O$, Showa Chemical Co. Ltd.], boron nitrade (BN, Sigma-Aldrich), isopropanol (C_3H_8O, Sigma-Aldrich), ethanolamine (C_2H_7NO, Alfa Aesar), which serve as base materials, dopant, solvent, and stabilizers, respectively. Acetic acid (CH_3COOH, Jingming Chemical CO., Ltd.), ethanol (CH_3CH_2OH, Reagent Duksan), acetonitrile (CH_3CN, JT Baker Avantor), potassium iodide (KI, Honeywell fluka), and iodine (I_2, Honeywell Fluka).

B-Doped ZnO Thin Films Synthesis

The deposition of ZnO thin films with various B-doped concentrations was carried out on indium tin oxide (ITO) glass substrate. The pristine ZnO film and boron nitride (BN)-doped samples with concentrations of 0, 1, 3, 5, and 7 wt% were labelled as ZO, ZOB-1, ZOB-3, ZOB-5, and ZOB-7, respectively. The sol-gel was synthesized using a modified reflux method. Zn and B precursors were dissolved in 50 mL of isopropanol under vigorous stirring for 10 minutes. Subsequently, 1.76 mL of ethanolamine was introduced dropwise into the solution as a stabilizer, and stirring continued for 3 h under reflux conditions. The resulting mixture was next transferred into a preheated 100 mL beaker to maintain thermal stability and facilitate evaporation. Within 30 minutes, the solution transformed into a viscous brown sol-gel, was deposited dropwise onto the ITO glass substrate, and spun at 5000 rpm. The sample was then dried at ambient conditions overnight. Thermal treatment involved a two-step annealing process: pre-heating at 250 °C for an hour and post-heating at 500 °C for 5 h.

Dye-Sensitized Solar Cell (DSSC) Fabrication

A natural dye was extracted from purple sweet potato (*Ipomoea batatas L.* Approximately 40 g of *Ipomoea batatas L.* was cut into small sizes, which were then ground with a mortar until softened and put into a sealed beaker glass with aluminum foil that contained DI water (16 mL), ethanol (30 mL), and acetic acid (4 mL). The mixture was stirred until homogeneously mixed and stored in a dark place for 24 h. The homogeneous dye was filtered and ready to use. These pristine ZnO and varied concentration B-doped ZnO thin films were immersed in a dye solution for 1 h to enable adsorption. After sensitization, the dye-covered films were washed sequentially with DI water and ethanol to remove unbound dye, followed by drying at ambient temperature. A platinum-deposited thin film on ITO served as a counter electrode, which was coated using a sputtering technique under an applied current of 20 mA for 40 s. The electrolyte solution comprises 0.5 M KI and 0.1 M I_2 in 10 mL CH_3CN.

Characterization Techniques

The crystallographic phases were examined using an X-ray diffractometer (XRD Bruker D2 Phaser 2nd generation) utilizing a monochromatic Cu Kα radiation (λ = 1.5418 Å). A field emission scanning electron microscope (FE-SEM JEOL7900F, 15 kV accelerating voltage) was used, providing energy dispersive X-ray spectroscopy (EDS) for surface morphology and elemental scanning, respectively. A UV-Vis spectrophotometer (Jasco V-770) was employed to analyze both absorbance and transmittance spectra. Potentiostat (SP-300) and UV lamp (36.5 watt) were utilized to analyze the J-V curves response towards the efficiency of pristine ZnO (ZO) and BN-doped ZnO (ZOB) thin films.

RESULTS AND DISCUSSION

X-ray Diffraction (XRD) Analysis

XRD analysis was utilized to identify the crystal structure of the as-fabricated ZO and ZOB-1 to ZOB-7 thin films. The XRD patterns in Fig.-1 provide a clear peak corresponding to the hexagonal wurtzite structure of ZnO, consistent with the standard JCPDS card number 36-1451. All samples demonstrate the presence of this crystalline phase, with a dominant diffraction peak observed along the (101) plane, indicating a preferential orientation of crystal growth. However, the pristine ZnO (ZO) and the B-doped (ZOB-1 to ZOB-7) thin films differ significantly. As illustrated in the zoomed-in 2θ 25.0° up to 28.5° of Fig.-1, the intensity of the appearing peak constantly increases as the B concentration rises. This indicates the disruption of the ZnO crystal structure due to the replacement of B atoms. B atoms, which have a smaller atomic radius than Zn atoms, tend to substitute for Zn atoms in the crystal lattice.[6,14] This substitution results in internal forces and lattice strain, which limit crystal growth and decrease crystal size.

Furthermore, the decrease in diffraction peak intensity and peak broadening indicates lattice distortion and crystal defect formation in response to the higher B doping concentration (notably in ZOB-5 and ZOB-7). These defects can serve as nucleation centers for forming new crystals but may also inhibit the growth of existing crystals. Consequently, the crystal size becomes smaller, and the crystal size distribution becomes wider. The XRD data reveal a gradual increase in the FWHM and a decrease in peak intensity of the ZnO diffraction peaks as the B concentration increases.

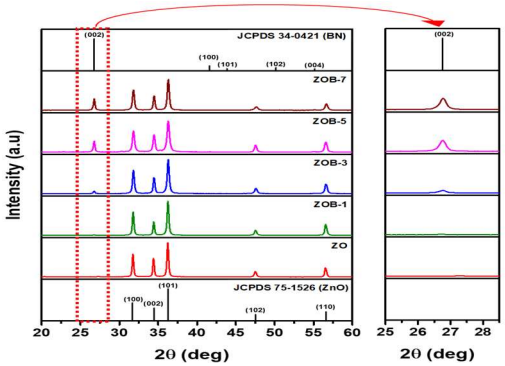

Fig.-1: X-ray Diffraction Patterns of ZO, ZOB-1, ZOB-3, ZOB-5, and ZOB-7 with the Zoomed-In Region at 2θ of 25.0° up to 28.5°

Table-1 presents the crystal sizes calculated from the (101) peak using the Scherrer equation, revealing a consistent decrease in crystal size with higher B doping concentrations. The Scherrer equation below was used to compute the crystal size of the ZO and ZOB-1 to ZOB-7:

$$D = \frac{0.9\lambda}{\beta \cos\theta_{(101)}} \qquad (1)$$

This trend aligns with previous studies, which report that increased B doping leads to inhibited crystal growth due to enhanced defect formation and lattice distortion.[14,15]

Table-1: The Crystal Size of ZO, ZOB-1, ZOB-3, ZOB-5, and ZOB-7 Thin Films

Samples	Peak (101)		Crystal Size (nm)
	2θ (deg)	FWHM (deg)	
ZO	36.8	0.247	37.5
ZOB-1	36.8	0.248	36.1
ZOB-3	36.8	0.285	31.5
ZOB-5	36.8	0.322	27.8
ZOB-7	36.8	0.348	26.7

Scanning Electron Microscopy (SEM) Analysis

SEM analysis was utilized to observe the surface morphology of the ZO and ZOB-1 to ZOB-7 thin films. As illustrated in Fig.-2, the addition of B notably alters the surface structure of the films. Fig.-2a shows that the surface of the ZO film has a homogeneous grain distribution and is smooth. The small grain size facilitates atomic diffusion, enabling grain coalescence and neck formation that reduce grain boundaries and lead to a smoother film surface. However, with the addition of B, the surface morphology transforms significantly. A low-B concentration of 1 wt% (ZOB-1) modifies the surface morphology, making it porous and granular. As depicted in Fig.-2b, the crystal grains uniformly agglomerate to form worm-like microscopic particles approximately 2 μm in size. Increasing the B concentration to 3 wt% (ZOB-3) leads to further morphological changes to flake-like particles, which grow larger than the ZOB-1, as shown in Fig.-2c. At 5 wt% B-doped concentration (ZOB-5) in Fig.-2d, the flake particles are smaller in size than the 3 wt% B-doped sample. When the B-doped amount reaches 7 wt% (ZOB-7) in Fig.-2e, a distinct flake-like morphology covering the underlying worm-like formations is observed. This suggests a saturation level of B doping, where further addition promotes greater agglomeration of ZOB particles. These SEM results correlate with the XRD results, which indicate that the worm-like and flake-like structures shown in Fig.-2 can be attributed to crystal defects and second phases detected at 2θ of 31.7° in the XRD pattern in Fig.-1.

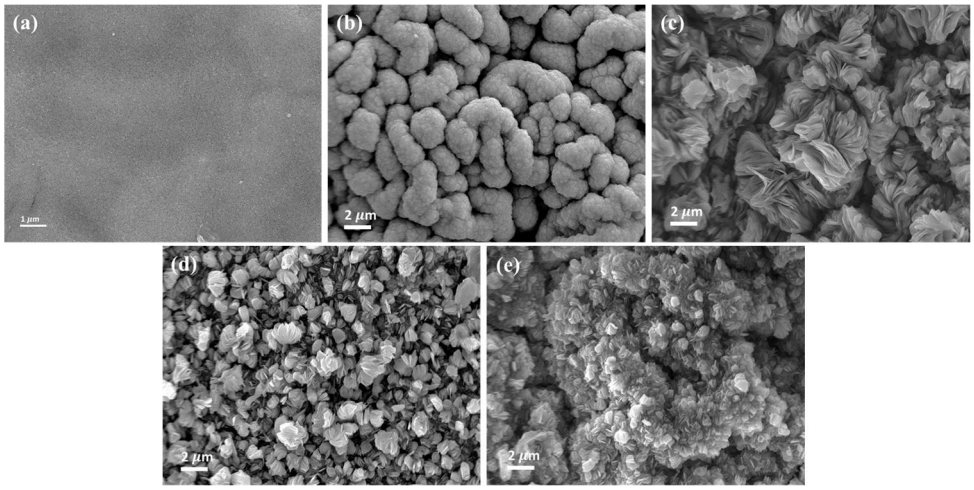

Fig.-2: SEM Images of (a) ZO, (b) ZOB-1, (c) ZOB-3, (d) ZOB-5, and (e) ZOB-7 Thin Films

Energy Dispersive Spectroscopy (EDS) Analysis

The elemental composition of ZO and ZOB-1 to ZOB-7 thin films was confirmed using EDS analysis. The EDS spectra in Fig.-3 identify peaks corresponding to O and Zn. A strong peak at 2 keV corresponds to the Pt layer, which was deposited to protect the sample from high accelerating voltage and enhance the conductivity. In contrast, the intensities of the O and Zn peaks gradually decrease, indicating the substitution of O and/or Zn atoms by B. However, the B peaks are not distinctly visible in the spectra. This is due to two key reasons: (1) the low atomic number of B (Z = 5), which results in weak interaction with the incident electron beam, and (2) very low X-ray emission energy (Kα = 0.183 KeV), making it difficult to distinguish from the background noise in the EDS spectrum. These limitations, combined with the inherent detection threshold of EDS for light elements, particularly at low energies, further contribute to the weak visibility of B peaks. These EDS results support the XRD findings, confirming that B is successfully incorporated into the ZnO lattice despite its low detectability in the EDS spectra. The O, B, and Zn atomic percentages in the ZO and ZOB-1 to ZOB-7 thin films are shown in Table-2. These results confirm that the B-doped concentration increases while the relative amounts of Zn and O decrease, consistent with the predetermined doping ratio. The Zn atomic percentage gradually decreases from 49.71% (ZO) to 45.05% (ZOB-7), while the O atomic percentage decreases slightly from 50.29% to 47.88%, respectively. Simultaneously, the B atomic percentage progressively increases from 0.87% (ZO) to 7.07% (ZOB-7), confirming the effective incorporation of B into the ZnO matrix. The integration of B atoms into the ZnO lattice leads to the formation of vacancies and strain-induced modifications, which play a key role in altering the physical and electronic properties of the ZnO lattice.

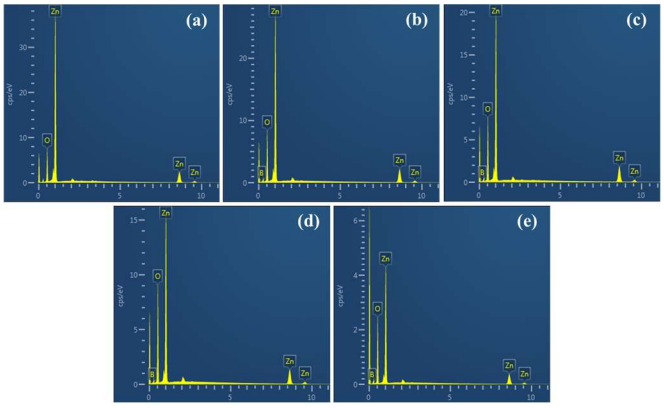

Fig.-3: The EDS Spectra of (a) ZO, (b) ZOB-1, (c) ZOB-3, (d) ZOB-5, and (e) ZOB-7 Thin Films

Table-2: The Atomic Percentages of ZO and ZOB-1 to ZOB-7 Thin Films

Samples	Elements		
	Zn	O	B
ZO	49.71	50.29	0.00
ZOB-1	48.14	50.99	0.87
ZOB-3	47.00	50.11	2.89
ZOB-5	46.56	48.59	4.85
ZOB-7	45.05	47.88	7.07

Ultraviolet Visible (UV-Vis) Spectrophotometer Analysis

Fig.-4 represents the UV-Vis spectrophotometer analysis was performed to examine the absorbance and transmittance spectra of each sample in the visible spectrum range of 300-700 nm. In Fig.-4a, all samples doped with B revealed changes in optical properties, as represented by a sharp drop in absorbance values in the UV wavelength, within the range of approximately 350-400 nm. The entire spectrum formed is nearly identical to the ultraviolet absorption region from a wavelength of 300-370 nm.[16] This indicates that the absorption edge is shifted toward lower wavelengths upon B doping. In the transmittance spectra presented in Fig.-4b, the ZO thin film exhibits a transmittance value of around 72%. For the ZOB-7 thin film, a slight rise in transmittance is observed at a wavelength of ~438 nm, about 73%. However, a general trend of decreasing transmittance in response to the higher B content is evident, particularly at higher doping levels (ZOB-5 and ZOB-7), which aligns with previously reported studies.[17,18] At lower B doping amounts (ZOB-1 and ZOB-3), the transmittance curves remain relatively smooth, and the films maintain a balance between optical absorption and transparency. These doping amounts appear to enhance light absorption without significantly compromising transmittance. In contrast, higher B concentrations (ZOB-5 and ZOB-7) result in irregularities or oscillations in the transmittance spectra, particularly between 370 and 470 nm. These spectral fluctuations can be attributed to increased structural disorder and crystal defects, which are also responsible for enhanced surface roughness and light scattering.[19] This means that the B-doped ZO thin film has increased light scattering on the surface. According to the Tauc plot (Eq. 2),[20] Which demonstrates the relation between absorption and photoenergy, the samples' direct band gap values were further calculated to determine the influence of B-doped content on the optical characteristics of ZO thin films.

$$(\alpha h\nu)^2 = C_D\left(h\nu - E_{opt}\right) \qquad (2)$$

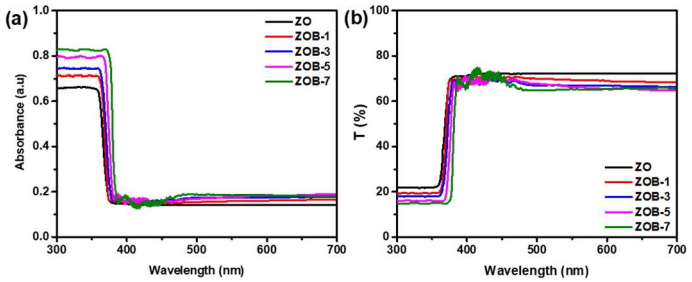

Fig.-4: The Optical Properties: (a) Absorbance, and (b) Transmittance (T%) spectra of ZO, ZOB-1, ZOB-3, ZOB-5, and ZOB-7 Thin Films

Band-gap Calculation

Fig.-5 demonstrates the Tauc plots, representing the $(\alpha h\nu)^2$ as a function of photon energy ($h\nu$). The linear region is extended to the x-axis to determine the band gap energy (Eg). B-doped in ZO thin films significantly alter their energy band gap, as shown in Table-3. The measured band gap values exhibit a decreasing trend from 3.37 eV (ZO) to 3.28 eV (ZOB-7), which can be attributed to structural defects and disorder states.[21] As depicted in Fig.-5, this band gap reduction is linked to defect states and increased dislocation density. A higher dislocation density narrows the atomic spacing, modifies the electronic band structures and consequently reducing the band gap.[22] Furthermore, elevated B doping concentrations promote greater nucleation sites, leading to intrinsic stress within the thin film and disrupting the ZnO host lattice.[23] The substitution of B atoms (B^{3+}, atomic radius: ~0.23 Å) for Zn atoms (Zn^{2+}, atomic radius ~0.74 Å) introduces lattice distortion due to the atomic size mismatch. This distortion alters the electron energy levels, requiring higher energy to excite electrons from the valence band to the conduction band. This

phenomenon is likely due to excessive lattice disorder, which disrupts the regular arrangement of the atoms in the crystal lattice and creates defect states inside the band gap. These defect states allow electronic transitions at lower energies, making the optical band gap smaller.

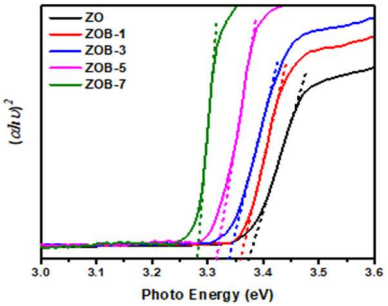

Fig.-5: The Energy Band Gap Curves of ZO, ZOB-1, ZOB-3, ZOB-5, and ZOB-7 Thin Films

Table-3: Band Gap Energy Values of ZO, ZOB-1, ZOB-3, ZOB-5, and ZOB-7 Thin Films

Samples	Band Gap (eV)
ZO	3.37
ZOB-1	3.36
ZOB-3	3.33
ZOB-5	3.31
ZOB-7	3.28

Efficiency

The current-voltage (J-V) measurements of the DSSCs are shown in Fig.-6. The J-V curves demonstrate the influence of B incorporation on the photovoltaic performance of ZO thin film. From the graph, it is evident that the ZO thin film (black curve) exhibits a good benchmark current density at 0 V, approximately 1.61 mA/cm^2. As B doping increases to 1% (ZOB-1 with the red curve), the current density reaches 1.82 mA/cm^2, indicating enhanced charge carrier generation and improved conductivity. A slight improvement is also observed for 3% (ZOB-3 with the blue curve), reaching 1.65 mA/cm^2, although it remains lower than ZOB-1. However, at higher doping concentrations of 5 wt% and 7 wt% (ZOB-5 and ZOB-7 with pink and green curves, respectively), the current density declines, suggesting the adverse effect of excessive B doping.

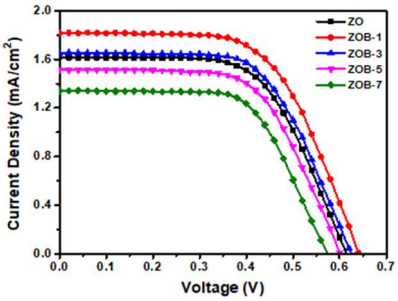

Fig.-6: *J*-V Curves Measurement for the as-Fabricated DSSCs Based on ZO, ZOB-1, ZOB-3, ZOB-5, and ZOB-7 Thin Films

This reduction could be attributed to increased defect states, charge carrier scattering, or potential structural distortions that hinder efficient charge transport. These findings highlight that moderate B doping (1–3%) enhances electrical properties, whereas higher concentrations (>5%) may introduce non-radiative recombination centers, leading to performance degradation. Table-4 displays the DSSCs' open circuit voltage (V_{OC}), short circuit current (J_{sc}), maximum power (P_m), fill factor (FF), and efficiency (η). Pristine ZnO as a benchmark exhibited a good P_{max} and η of 0.6 W/cm^2 and 1.64%, respectively. The V_{OC}, J_{SC}, and P_{max} for ZOB-1 to ZOB-7 show the identical trend which decreases as the B doping concentration increases, leading to a dramatic reduction of DSSC η from 1.91% to 1.35%. Compared to the ZO, ZOB-1 achieved better performance in the DSSC application. The reduction of J_{sc} is related to the decrease in the

transmittance value and causes a gradual narrowing of the band gap energy, which could hinder light absorption, and reduce dye excitation, resulting in fewer electrons being injected into the conduction band of ZnO and reduced efficiency.[24] Therefore, these findings confirm that controlled B doping, particularly at 1 wt%, effectively enhances the structural and optoelectronic properties of ZnO thin films, making them promising candidates for high-efficiency DSSC photoanodes.

Table-4: Performance Parameters for the As-Fabricated DSSCs of ZO, ZOB-1, ZOB-3, ZOB-5, and ZOB-7 Thin Films

Samples	V_{OC} (V)	J_{SC} (mA/cm^2)	P_{max} (W/cm^2)	FF (%)	η (%)
ZO	0.61	1.61	0.60	60.9	1.64
ZOB-1	0.64	1.82	0.70	60.2	1.91
ZOB-3	0.62	1.65	0.63	61.3	1.72
ZOB-5	0.60	1.51	0.56	61.8	1.53
ZOB-7	0.57	1.34	0.49	64.1	1.35

CONCLUSION

The ZO thin film with varying B doping concentrations from 1 up to 7 wt% was properly synthesized via the sol-gel spin-coating technique, resulting in a hexagonal wurtzite crystal structure. The integration of B atoms into the ZnO lattice introduced controlled defect states, leading to the formation of two distinct structural phases, increased surface roughness, and reduced grain size. This increased roughness promoted incident light scattering, subsequently reducing optical transmittance. As a result, the energy band gap decreased, which could negatively impact DSSC efficiency. In particular, the ZOB-1 was identified as the the optimal doping concentration to enhance the efficiency of DSSC. Conversely, higher doping concentration (ZOB-3 to ZOB-7) introduced excessive defects that degraded device performance. Overall, these findings confirm that low-level of 1 wt% B doping concentration is a viable strategy for enhancing ZnO-based photoanodes in DSSC applications.

ACKNOWLEDGMENTS

The authors would like to thank the Chancellor and the Head of the Institute for Research and Community Service, Universitas Negeri Medan, for the support through PNBP funding under Grant No. 0236/UN33.8/PPKM/PPT/2024.

CONFLICT OF INTERESTS

The authors declare that there is no conflict of interest.

AUTHOR CONTRIBUTIONS

The present work is related to *SDG-7: Affordable and Clean Energy*. All the authors contributed significantly to this manuscript, participated in reviewing/editing, and approved the final draft for publication. The research profile of the authors can be verified from their ORCID ids, given below:

Nurdin Siregar http://orcid.org/0000-0001-8227-5582
Motlan http://orcid.org/0000-0002-6246-0032
Makmur Sirait http://orcid.org/0000-0002-1400-6708

Open Access: This article is distributed under the terms of the Creative Commons Attribution 4.0 International License (http://creativecommons.org/licenses/by/4.0/), which permits unrestricted use, distribution, and reproduction in any medium, provided you give appropriate credit to the original author(s) and the source, provide a link to the Creative Commons license, and indicate if changes were made.

REFERENCES

1. I. Arora, H. Chawla, A. Chandra, S. Sagadevan and S. Garg, *Inorganic Chemistry Communications*, **143** 109700(2022), https://doi.org/10.1016/j.inoche.2022.109700
2. Z. Paltusheva *et al.*, *Physical Sciences and Technology*, **11(1-2)**, (2024), https://doi.org:10.26577/phst2024v11i1a6
3. N. Siregar, Motlan and J. Panggabean, *Journal of Physics: Conference Series*, **1428(1)**, 012026(2020), https://doi.org:10.1088/1742-6596/1428/1/012026

4. M. Sharmin and A. H. Bhuiyan, *Journal of Materials Science: Materials in Electronics*, **30(5)**, 4867(2019), https://doi.org:10.1007/s10854-019-00781-8
5. S. R. Bhattacharyya, Z. Mallick and R. N. Gayen, *Journal of Electronic Materials*, **49(6)**, 3860(2020), https://doi.org:10.1007/s11664-020-08107-9
6. B. Wen *et al.*, *Applied Physics A*, **123(3)**, 211(2017), https://doi.org:10.1007/s00339-017-0847-z
7. S. S. S. Al-Qadasy, H. Q. N. M. Al-Arique, N. M. S. Kaawash, S. Q. Chishty and K. A. Bogle, *Physica Scripta*, **99(6)**, 0659a3(2024), https://doi.org:10.1088/1402-4896/ad4b73
8. I. K. Abd, F. H. Abdulrazzak and Z. T. Khodair, in AIP Conference Proceedings, https://doi.org:10.1063/5.0000033
9. S. Sha *et al.*, *Colloids and Surfaces A: Physicochemical and Engineering Aspects*, **630**, 127491(2021), https://doi.org/10.1016/j.colsurfa.2021.127491
10. M. Z. Silitonga, N. S. Gultom and D.-H. Kuo, *Applied Surface Science*, **655**, 159651(2024), https://doi.org/10.1016/j.apsusc.2024.159651
11. V. T. Lukong, K. Ukoba and T.-C. Jen, *The International Journal of Advanced Manufacturing Technology*, **122(9)**, 3525(2022), https://doi.org:10.1007/s00170-022-10043-3
12. E. S. Teixeira *et al.*, *Materials Research*, **23(6)**, (2020), https://doi.org/10.1590/1980-5373-MR-2020-0214
13. A. Atılgan and K. Özel, *Gazi University Journal of Science Part A: Engineering and Innovation*, **11(1)**, 57(2024), https://doi.org:10.54287/gujsa.1362103
14. B. Wen *et al.*, *Chemical Research in Chinese Universities*, **30(3)**, 509(2014), https://doi.org:10.1007/s40242-014-3497-0
15. S. Sushama, P. Murkute, H. Ghadi, S. K. Pandey and S. Chakrabarti, *Journal of Luminescence*, **238**, 118221(2021), https://doi.org/10.1016/j.jlumin.2021.118221
16. Z. Hu *et al.*, *ACS Applied Materials and Interfaces*, **12(5)**, 5979(2020), https://doi.org:10.1021/acsami.9b21628
17. A. M. Alsaad, A. A. Ahmad, I. A. Qattan, Q. M. Al-Bataineh and Z. Albataineh, *Crystals*, **10(4)**, 252(2020), https://doi.org/10.3390/cryst10040252
18. A. M. Alsaad, Q. M. Al-Bataineh, A. A. Ahmad, Z. Albataineh and A. Telfah, *Optik*, **211**, 164641(2020), https://doi.org/10.1016/j.ijleo.2020.164641
19. T. Hurma, *Journal of Molecular Structure*, **1189**, 1(2019), https://doi.org/10.1016/j.molstruc.2019.03.096
20. H. Abdullah, Y.-R. Ko, D.-H. Kuo and N. S. Gultom, *ACS Applied Materials and Interfaces*, **12(14)**, 16186(2020), https://doi.org:10.1021/acsami.9b19885
21. A. A. Ahmad, A. M. Alsaad, Q. M. Al-Bataineh and M. A. Al-Naafa, *Applied Physics A*, **124(6)**, 458(2018), https://doi.org:10.1007/s00339-018-1875-z
22. Z. N. Kayani, Z. Bashir, S. Riaz, S. Naseem and Z. Saddiqe, *Journal of Materials Science: Materials in Electronics*, **31(14)**, 11911(2020), https://doi.org:10.1007/s10854-020-03745-5
23. B. Pejjai, V. R. M. Reddy, K. Seku, T. R. R. Kotte and C. Park, *Optik*, **130**, 608(2017), https://doi.org/10.1016/j.ijleo.2016.10.083
24. S. Baruah, R. A. Afre and D. Pugliese, *Energies*, **17(9)**, 2076(2024), https://doi.org/10.3390/en17092076

[RJC-9295/2025]